Simulated multileaf collimator tracking for stereotactic liver radiotherapy guided by kilovoltage intrafraction monitoring: dosimetric gain and target overdose trends

Per R Poulsen[a,b], Ghulam Murtaza[a,c], Esben S Worm[d], Thomas Ravkilde[d], Ricky O'Brien[e], Cai Grau [a,b], Morten Høyer[b] and Paul Keall[e]

[a]Department of Oncology, Aarhus University Hospital, Aarhus, Denmark

[b]Danish Center for Particle Therapy, Aarhus University Hospital, Aarhus, Denmark

[c]School of Health Sciences, University of Management & Technology, Lahore, Pakistan

[d]Department of Medical Physics, Aarhus University Hospital, Denmark

[e]ACRF Image X Institute, Sydney Medical School, University of Sydney, Sydney, NSW, Australia

Corresponding author:
Per Rugaard Poulsen
Department of Oncology and Danish Center for Particle Therapy
Aarhus University Hospital
Palle Juul-Jensens Boulevard 25, Entrance B3, 8200 Aarhus N, Denmark
Tel: +4578462651
Fax: +4578464522
Email: per.poulsen@rm.dk

Number of pages: 20
Number of tables: 0
Number of figures: 6
Running head: KIM-guided MLC tracking for liver SBRT

Key words: Image-guided radiation therapy; radiotherapy target organ alignment; intrafraction motion; kilovoltage intrafraction monitoring; multileaf collimator tracking

Highlights

- Tumor motion during liver SBRT can compromise the tumor dose
- KIM-guided MLC tracking can restore the tumor dose coverage
- Tumor motion perpendicular to the MLC leaves can create dose hotspots in the tumor

Abstract

Purpose: To investigate the potential benefit of multileaf collimator (MLC) tracking guided by kilovoltage intrafraction monitoring (KIM) during stereotactic body radiotherapy (SBRT) in the liver, and to understand trends of target overdose with MLC tracking.

Methods: Six liver SBRT patients with 2-3 implanted gold markers received SBRT delivered with volumetric modulated arc therapy (VMAT) in three fractions using daily cone-beam CT setup. The CTV-to-PTV margins were 5 mm in the axial plane and 10 mm in the cranio-caudal directions, and the plans were designed to give minimum target doses of 95% (CTV) and 67% (PTV). The three-dimensional marker trajectory estimated by post-treatment analysis of kV fluoroscopy images acquired throughout treatment delivery was assumed to represent the tumor motion. MLC tracking guided by real-time KIM was simulated. The reduction in CTV D95 (minimum dose to 95% of the clinical target volume) relative to the planned D95 (ΔD95) was compared between actual non-tracking and simulated MLC tracking treatments.

Results: MLC tracking maintained a high CTV dose coverage for all 18 fractions with ΔD95 (mean: 0.2 percentage points (pp), range: -1.7-1.9 pp) being significantly lower than for the actual non-tracking treatments (mean: 6.3 pp range: 0.6-16.0 pp) ($p=0.002$). MLC tracking of large target motion perpendicular to the MLC leaves created dose artifacts with regions of overdose in the CTV. As a result, the mean dose in spherical volumes centered in the middle of the CTV was on average 2.4 pp (5mm radius sphere) and 1.3 pp (15mm radius sphere) higher than planned ($p=0.002$).

Conclusions: Intrafraction tumor motion can deteriorate the CTV dose of liver SBRT. The planned CTV dose coverage may be restored with KIM-guided MLC tracking. However, MLC tracking may have a tendency to create hotspots in the CTV.

Introduction

Stereotactic body radiation therapy (SBRT) emerged a quarter of a century ago (1,2) and has recently seen increased interest for both metastases (3) and primary tumors in the liver (4). With few fractions and steep dose gradients the treatments should be delivered as accurately as possible, but motion during liver SBRT is a challenge that may compromise the tumor dose (5-7).

A high treatment accuracy in the presence of tumor motion may be obtained by real-time tumor tracking with the robotic CyberKnife system (8) or the gimbaled Vero system (9), which are however highly specialized treatment machines. A potential alternative approach on a conventional linear accelerator is multileaf collimator (MLC) tracking, where the MLC aperture is adjusted continuously to follow the tumor motion. In the first clinical trials, real-time tumor localization by implanted electromagnetic transponders was used to guide prostate (10) and lung (11) cancer MLC tracking. In a recent prostate cancer trial, MLC tracking was integrated with kilovoltage intrafraction monitoring (KIM), where the three-dimensional (3D) real-time target position signal is supplied by x-ray imaging perpendicular to the treatment beam (12). A useful feature of KIM-guided MLC tracking is that the real-time target localization and motion adaptation only rely on a gantry-mounted kV imager and an MLC, which are both standard equipment of modern conventional linear accelerators. With no additional hardware costs, this tracking method has large potential for widespread use.

A future clinical application of MLC tracking is for liver SBRT, where drift and respiratory motion can be large and cause substantial tumor dose reductions in treatments without real-time motion adaptation (5,6). Retrospective KIM of implanted marker motion during volumetric modulated radiotherapy

(VMAT) delivery in the liver has shown sub-millimeter localization accuracy (5), but so far KIM-guided MLC tracking has not been investigated for liver SBRT. Due to the large tumor motion it is important to establish the accuracy of MLC tracking for liver SBRT. In this study, we use kV images acquired during liver SBRT treatments to perform realistic simulations of KIM-guided MLC tracking. We use dose reconstruction with and without the simulated MLC tracking to quantify the dosimetric gain of the tracking. The MLC tracking doses provide new and valuable information on systematic tendencies that MLC tracking can have to create dose hotspots in the target.

Materials and methods

Patients, planning and imaging

This study includes the same six liver SBRT patients as Ref. (5), where the planned tumor doses in VMAT treatments (Figure 1, upper row) were compared with the actually delivered doses as reconstructed by use of the 3D tumor motion during treatment delivery (Figure 1, middle row). The patients had one (n=3), two (n=1), four (n=1) or six (n=1) metastases and 2-3 gold markers implanted close to the metastases. Delineation of the lesions in the mid-ventilation phase of a 4DCT scan formed both the gross tumor volume (GTV) and the clinical target volume (CTV). Following our institutional standard, the CTV was extended by 5mm margins in the left-right (LR) and anterior-posterior (AP) directions and 10mm margins in the cranio-caudal (CC) direction to generate the planning target volume (PTV) (13). VMAT plans with 5-6 arcs covered the CTV with 95% and the PTV with 67% of the prescribed mean CTV dose, which was 56.25Gy (n=2) or 75Gy (n=4) in three fractions. The patients were treated on Trilogy accelerators with Millennium MLCs (Varian Medical Systems, Palo Alto, CA) using a flattening filter and a nominal dose rate of 600 MU per minute. Abdominal compression was used for all patients. During treatment delivery, fluoroscopic kV images were acquired perpendicular to the treatment beam with 5Hz frequency. After the treatments, the gold marker closest to the isocenter was segmented in the kV images and its 3D motion was estimated from the projected 2D motion with the probability-based method of

KIM (14). Analysis of continuous portal images from the treatments showed that the post-treatment 3D motion estimation by KIM had sub-millimeter accuracy (5). In the current study, we therefore use this motion as the actual ground truth tumor motion in the simulated treatments. Over all fractions the mean (and range) of the peak-to-peak tumor motion per fraction was 4.8mm (2.1-8.7mm) (LR), 16.2mm (7.3-35.4mm) (CC) and 6.4mm (2.0-9.7mm) (AP). More details on the patients, treatments, tumor motion and KIM imaging dose can be found in Ref. (5).

MLC tracking simulations

KIM-guided MLC tracking treatments on a Trilogy accelerator was simulated for all fractions (Figure 1, bottom row). Since the jaws are static during MLC tracking on a Trilogy accelerator the jaw positions of each VMAT field was extended 15mm and the positions of all closed MLC leaf pairs were moved behind the new jaw positions to allow MLC aperture shifts within the fixed jaw-defined field. Due to large field sizes this procedure was not possible for the two patients with four or six metastases. Therefore, new VMAT plans with the original collimator and gantry angles, but only covering the largest metastasis, were made for these patients. After jaw extension all plans were recalculated and renormalized to CTV mean doses of 100%. It should be noted that the plans were not originally designed for MLC tracking. In clinical VMAT MLC tracking of respiratory motion, the MLC leaves are typically aligned along the CC direction (11). However, for the 31 VMAT fields in this study, the MLC leaves were rotated 30° (n=4), 45° (n=12), 60° (n=4), or more (n=11) from the CC direction.

The MLC tracking treatments were simulated with in-house developed software similar to the TrueBeam tracking simulator described in Ref (15), but optimized to simulate MLC tracking on a Trilogy accelerator and with the capability to emulate real-time tumor localization by KIM. In accordance with Ref. (16) the MLC leaf adjustment to a requested step Δx was assumed to last 56ms for $\Delta x < 1.3$mm and to occur with 22ms latency followed by leaf motion at 3.8cm/s for $\Delta x \geq 1.3$mm. Trilogy MLC tracking (17) differs from TrueBeam MLC tracking (18) by a higher maximum MLC leaf speed (3.8cm/s (16) versus 2.5 cm/s (18)) and a different

prediction algorithm (kernel density estimation predictor (19) versus linear Kalman filter prediction (18)), and by having static rather than tracking jaws during MLC tracking. Trilogy MLC tracking has been integrated with a wide range of real-time localization methods, including KIM (17), while TrueBeam MLC tracking has been integrated with optical monitoring and electromagnetic monitoring, only (18).

The width of the aperture-forming MLC leaves was 5mm. The tracking simulations assumed kV imaging at the same time points and with the same 2D marker positions in the images as in the actual clinical treatments. Real-time KIM estimation of the 3D marker position of the latest kV image was performed by first fitting a 3D Gaussian probability density function (PDF) to a series of previous images, including the latest image, and then estimating the 3D position as the most likely position given the projected 2D position and the 3D Gaussian PDF (14). In clinical real-time KIM treatments, kV images are acquired during a pre-treatment gantry rotation (20) or as part of a cone-beam CT scan (21) and used to build the PDF prior to treatment start. However, such pre-treatment kV images were not available in the current simulation study. Therefore, the 3D tumor position was not estimated by KIM until 90 images had been acquired during the first VMAT field of a fraction. In this initial period, the MLC tracking assumed perfect tumor alignment in the LR and AP directions and only compensated for the CC tumor motion, which was directly visible in the kV images. After acquisition of 90 kV images, the full 3D tumor position was estimated in real time by KIM and compensated by MLC tracking. At the subsequent fields, the PDF for KIM was estimated from the last 200 images of the preceding field and all images acquired so far during the current field. The KIM-guided MLC tracking has a system latency of 290ms (17), which was accounted for by the kernel density estimation-based prediction algorithm (19) used in a lung MLC tracking trial (11). The prediction started 8 seconds into the first field delivery when sufficient training data had been recorded.

Geometric and dosimetric delivery errors

For all simulated MLC tracking fractions, the root-mean-square (rms) error of the real-time tumor localization was calculated separately for the two steps of 3D position estimation by KIM and motion prediction as well as for the two steps combined. For all fractions, non-tracking and tracking, the time resolved tumor position error in beam's eye view (BEV) was calculated and its rms value was reported. It provided a geometric error quantity that was directly applicable to both non-tracking and MLC tracking treatments. For MLC tracking treatments, the BEV tumor position error at a time point was calculated as described in Ref. (7) as the difference between the current MLC aperture position and the ideal aperture, which was defined as the planned MLC aperture shifted in BEV to the current target position.

For all treatment fractions, motion-including tumor dose reconstruction was performed by dividing each VMAT beam into multiple sub-beams that were each given an isocenter shift that reflected the tumor position when the sub-beam was delivered (5,22). The sub-beam generation was performed in an in-house built Matlab program (version R2016a), while the dose of the motion-encoded plan was calculated in the treatment planning system (Eclipse, Varian Medical Systems). Rather than using the original clinical plans, the actually delivered dose without tracking was reconstructed using the tracking prepared plans with extended jaws and altered to irradiate only the largest metastasis for two patients. It allowed direct comparison between non-tracking and tracking doses. The motion-including doses were used to calculate the CTV ΔD95, i.e. the reduction in the minimum dose to 95% of the CTV relative to the planned dose. A two-sided Wilcoxon signed rank test was used to investigate for significant differences between CTV ΔD95 in non-tracking and MLC tracking treatments. Pearson's correlation coefficient was used to test for correlation between the BEV rms position error and CTV ΔD95 at a fraction.

In order to investigate potential trends in the dose as a function of distance from the center of the CTV all dose distributions were exported as Dicom dose files from the treatment planning system and analyzed in a Matlab program. A radial dose distribution was determined by calculating the mean dose in 1mm thick spherical shells with the same center as the CTV and increasing radii in steps of 1mm. Furthermore, the mean dose

delivered in spherical regions with 5mm, 10mm and 15mm radius and centered in the CTV center was compared with the planned dose using a two-sided Wilcoxon signed rank test.

Supplementary experiments

In order to investigate if experiments show similar dose error trends as the treatment simulations the dose errors of a recent experimental MLC tracking study (23) were investigated. Optically guided MLC tracking with a TrueBeam accelerator was performed with the treatment plan and tumor motion from one fraction for five of the six liver SBRT patients of the current simulation study (23). The dose distributions of tracking and non-tracking motion experiments as well as static reference experiments were measured for a total of 25 VMAT fields with a biplanar Delta4 dosimeter (Scandidos, Sweden). For each experiment, the radial dose distribution was extracted as described in the previous paragraph and the mean dose in spherical regions was compared between the motion experiments and static experiments.

Results

Figure 2 compares the real-time KIM estimated liver tumor motion with the actual motion for the first VMAT field at a treatment fraction. In the MLC tracking treatments, the LR and AP position was assumed to equal the planned position in the first 18s until 3D KIM localization was initiated after 90 kV images. The mean gantry rotation at all fractions before initiation of 3D real-time localization and MLC tracking in the LR and AP direction was 34° (range: 22-45°). In subsequent fields, 3D localization took place from the start of the field delivery. The 18s with only CC MLC tracking constituted 2.9-4.5% of the treatment delivery duration (3.9% in mean). After 8s treatment the prediction algorithm started to compensate for the tracking system latency. Irregular breathing occasionally caused substantial prediction errors, an example being after ~70s in Figure 2 where a breathing period longer than the preceding periods cause erroneous prediction. The mean rms error of the real-time tumor localization per fraction was 0.54mm (LR), 0.04mm (CC), and 0.52mm (AP) for the 3D

position estimation by KIM, 0.36mm (LR), 1.26mm (CC), and 0.50mm (AP) for the prediction, and 0.66mm (LR), 1.26mm (CC), and 0.72mm (AP) for both steps combined.

In BEV, a larger part of the tumor motion (53.2% variance) was perpendicular to the MLC leaves than parallel to the leaves (46.8% variance), reflecting that the collimator angle was not optimized for MLC tracking of liver tumor motion. The 2D rms tumor position error in BEV per fraction had a mean (range) of 4.5mm (2.4-6.4mm) without MLC tracking and 2.4mm (1.4-4.2mm) with MLC tracking.

Figure 3 presents the planned and delivered dose distributions accumulated over the 3-fraction course for the three patients whose CTV ΔD95 without MLC tracking was smallest (Patient 3), largest (Patient 5) and closest to the mean (patient 1). The dose distributions for the other three patients are shown in Supplementary Figure 1. For all patients, the CTV dose volume histogram (DVH) indicates the presence of CTV low dose regions without MLC tracking and hot spots with higher doses than planned with MLC tracking. MLC tracking was in general able to maintain a high CTV dose coverage as indicated by a mean CTV ΔD95 of 0.2 percentage points (pp) (range: -1.7-1.9 pp) for individual fractions. It was significantly lower than CTV ΔD95 without MLC tracking (mean: 6.3 pp, range: 0.6-16.0 pp) ($p=0.0002$). For the accumulated dose over the three-fraction treatment courses, the mean (and range) of CTV ΔD95 was 0.5 pp (-1.4-1.6 pp) with MLC tracking and 5.6 pp (0.7-11.9 pp) without tracking. CTV ΔD95 per fraction was highly correlated with the 2D rms error in BEV ($r=0.90$, $p<<0.0001$) (Figure 4).

At 9 out of 18 fractions, MLC tracking resulted in higher CTV D95 doses than planned (negative ΔD95 in Figure 4). The radial dose distributions showed that MLC tracking gave significantly higher doses than planned in the central part of the CTV (Figure 5). The mean dose was on average 2.4 pp (range: 1.2-4.4 pp, $p=0.0002$), 2.1 pp (1.1-3.9 pp, $p=0.0002$) and 1.3pp (0-3.1 pp, $p=0.0002$) higher than planned in central spherical regions of 5mm, 10mm and 15mm radius, respectively. Without tracking the mean dose in the same regions was on average 0.5 pp ($p=0.14$), 1.0 pp ($p=0.006$) and 2.0 pp ($p=0.002$) lower than planned.

Analysis of the target overdose trend of MLC tracking indicated that it was caused by the finite speed of the MLC leaves when they adjusted to tumor motion perpendicular to the MLC leaves in BEV. An intuitive explanation is illustrated in the top row in Figure 6. When the target moves one leaf width perpendicular to the MLC leaves, the adjustment of the MLC aperture to the new target position will in general involve extension of some leaves (indicated with red arrows in Figure 6) and retraction of some other leaves (blue arrows). The leaf extension takes a finite time during which the area not yet covered by the extending leaf is unintentionally exposed to radiation (red arrows in Figure 6a-c). These over-exposed areas will often be located in the central part of the MLC aperture since the extending leaf typically moves towards the center. Similarly, the area still covered by a retracting leaf will be under-exposed. The under-exposed areas will often be located in the periphery of the MLC aperture since the leaf typically retracts toward this region. The net result is a shift of dose from the periphery to the center of the MLC aperture caused by the finite leaf speed when the MLC aperture is adjusted to perpendicular target motion. Figure 6(d) shows the cumulative exposure error of the MLC adjustment in Figures 6(a-c). Similarly, Figure 6(e) presents the cumulative MLC exposure errors caused by MLC adjustments for the simulated MLC tracking treatments for the three patients in Figure 3. Corresponding figures for the three other patients are presented in Supplementary Figure 2. The figures show a clear systematic trend of overexposure in the central part of the MLC aperture and underexposure near the rim. The over-exposure in BEV in Figure 6(e) and Supplementary Figure 2 affected varying parts of the tumor during the tracking treatments due to gantry rotation during VMAT fields and collimator rotation between fields. The result was a tendency of hotspots in the CTV as seen in the MLC tracking dose distributions in Figure 3 and Supplementary Figure 1.

Supplementary Figure 3 shows the dose distributions measured for five of the six patients in static experiments along with the dose errors in motion experiments with and without MLC tracking. As reported in Ref. (23) MLC tracking largely improved the delivered dose distributions compared to non-tracking experiments. However, similarly to simulations MLC tracking resulted in overdosed regions within the target,

which is further illustrated by the radial dose distributions in Supplementary Figure 4. Averaged over all 25 VMAT fields in the experiments the mean dose with MLC tracking was 2.5 % (p =0.0003), 2.3 % (p =0.0001) and 1.9 % (p =0.0001) higher than in the static experiments in central regions of 5mm, 10mm and 15mm radius, respectively. This is summarized in Supplementary Table 1 along with separate statistics for fields with the MLC leaves rotated at most 45° from the CC direction and least 60° from the CC direction. For 15 fields with at least 60° leaf rotation, MLC tracking gave significantly higher mean doses than static treatments in all three spherical regions (p = 0.0002-0.0004). For 10 fields with at most 45° leaf rotation, MLC tracking gave significantly higher mean doses than static treatments in the 10mm radius region (p = 0.04), but not in the 5mm radius region (p = 0.11) nor 15mm radius region (p = 0.06) (Supplementary Table 1).

Discussion

Simulation of KIM-guided MLC tracking for six liver SBRT patients showed that the tracking can maintain a high tumor dose coverage even in the presence of large intrafraction motion that clearly reduced the tumor dose coverage without MLC tracking. KIM-guided MLC tracking has been implemented for prostate cancer (12) and may see widespread clinical use since it only requires software upgrades of standard-equipped conventional linear accelerators. It would allow reduction of motion margins and function as a safety belt that ensures high tumor dose coverage even for the patients with largest motion. The KIM imaging adds an effective dose per fraction that is comparable to the dose of a cone-beam CT scan (5).

A tendency of hotspots in the CTV with MLC tracking was observed and an intuitive explanation was given in terms of the finite leaf speed in MLC adjustments to perpendicular tumor motion. It stresses the need for proper selection of the collimator angle for MLC tracking of respiratory motion. MLC exposure errors during MLC tracking are not only caused by MLC adjustments, but are also due to real-time target localization errors and MLC leaf fitting errors (17). It is, however, only the MLC adjustment error that has the general tendency illustrated in Figure 6 to over-expose the central part of the MLC aperture increasing the CTV dose.

Investigation of previous MLC tracking experiments with the same treatment plans as in the simulations revealed a similar tendency of central overdose. This overdose was largest for treatment fields with largest MLC leaf rotation relative to the CC direction, supporting the assumption that it is caused by target motion perpendicular to the MLC leaves.

In the current study, we used the original clinical VMAT plans to allow direct comparison of MLC tracking with actual non-tracking treatments in our department. Therefore, the collimator angle was not optimized for MLC tracking. Alignment of the MLC leaves along the CC axis, which is standard for lung VMAT MLC tracking (11), would reduce the fraction of BEV target motion perpendicular to the MLC leaves from 53.2% of the target position variance to 20.3% of the variance. This would decrease the tendency of hotspots in the target. It has previously been shown that liver tumors in general have a dominant motion direction that can be estimated with good accuracy from a 4DCT scan (24). For the patients in this study, this could be exploited to further reduce the perpendicular tumor motion to 13.3% of the variance by VMAT plans with gantry dependent collimator angles that align the MLC leaves along the main motion direction (first principal component) of the 4DCT motion (25). The MLC exposure errors from MLC adjustment to perpendicular target motion may also be decreased by faster leaf motion or by reducing the leaf motion needed to adapt to perpendicular target motion. This can be obtained by designing less complex VMAT plans (26) or using the Y-jaws rather than the MLC leaves to define the field edges (27).

Despite the non-optimal collimator angles and lack of full 3D target localization in the first 18s of a treatment the MLC tracking ensured good target coverage for all treatment fractions in this study (Figure 4). Furthermore, the large target motion perpendicular to the MLC leaves gave new insight into systematic dosimetric errors with a net transport of dose from the periphery to the central part of the MLC aperture. The tendency of MLC tracking to create hotspots in the target region has been observed previously by other researchers, who did, however, not explain the underlying mechanism (28-29). In experiments comparing couch tracking with MLC tracking for prostate SBRT VMAT treatments with integrated boost, Ehrbar *et al*. found that

MLC tracking significantly increased the mean doses to the index lesions and the urethra (28). In a comparison between gating and MLC tracking for prostate, Colvill *et al*. showed examples of increased target doses with MLC tracking (see Figure 5 in Ref (29)). In this study, we could explain the trend of overdosing the target by MLC adjustments to target motion perpendicular to the MLC leaves. While the hotspots may be clinically acceptable for the SBRT treatments of the current study it will naturally be less acceptable for treatments with planned target dose inhomogeneities such as prostate plans with higher doses to index lesions or lower doses to the urethra.

MLC tracking of perpendicular target motion is discretized by the finite leaf width, and large leaf motion is sometimes needed to adapt to a small target motion. Couch tracking (28), robotic tracking (8) and gimbal tracking (9) do not have these limitations. On the other hand, only MLC tracking has the potential to adapt to target deformations and differential motion of multiple targets. Since the target motion is always known in tracking treatments motion-including dose reconstruction as in the current paper will in general be possible in order to examine whether the delivered dose is acceptable. With current developments in real-time dose reconstruction (30-31) this examination may even be performed online as the treatment is being delivered, which could enable improved MLC tracking with dose-guided MLC aperture adaptation.

In conclusion, simulations showed that KIM-guided MLC tracking can restore the planned tumor dose coverage in liver SBRT, but tumor motion perpendicular to the MLC leaves can create a tendency of target overdose due to the finite MLC adjustment speed.

Acknowledgements

This study was supported by the Danish Cancer Society and Danish Comprehensive Cancer Center Radiotherapy - The Danish National Research Center for Radiotherapy.

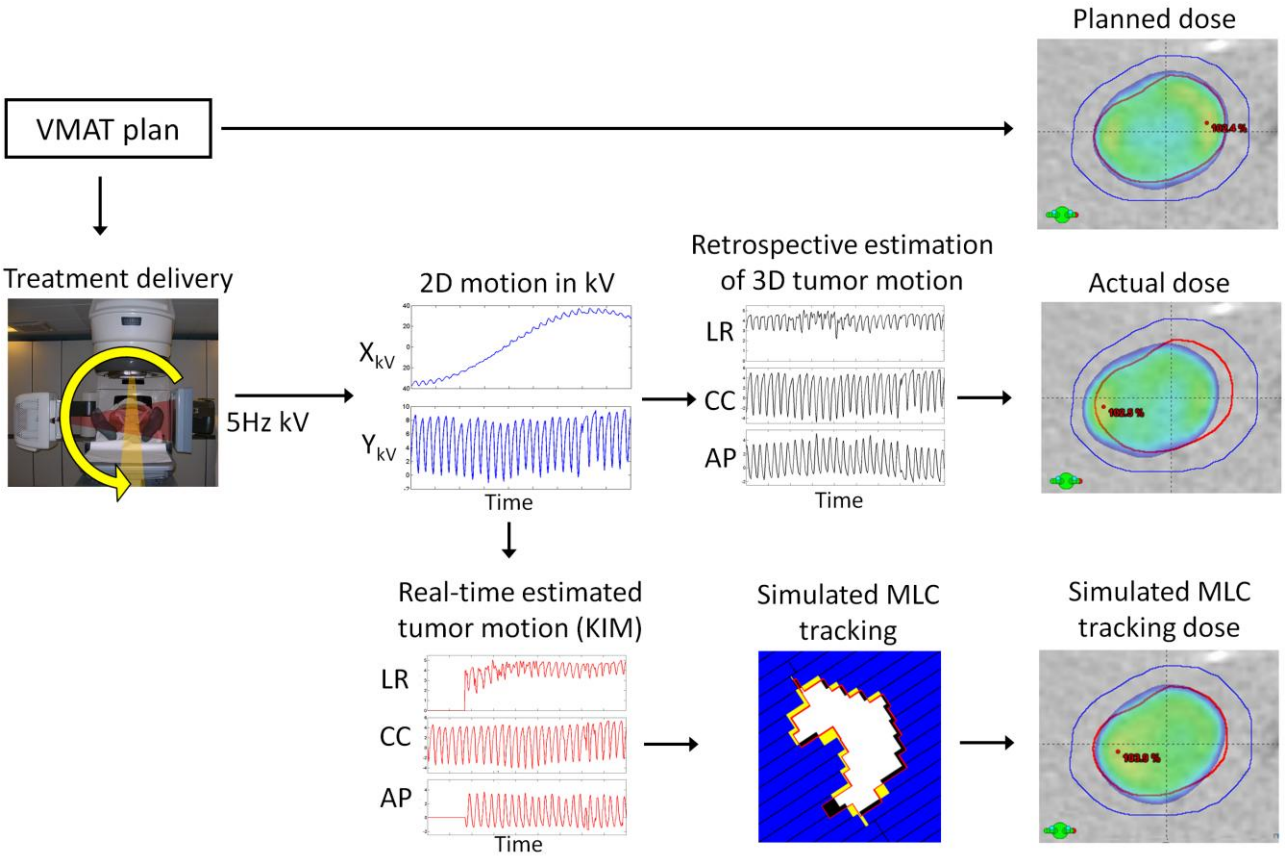

Figure 1. Method overview. For each VMAT treatment, the actually delivered dose without real-time motion adaptation (middle row) and the dose of simulated MLC tracking guided by real-time kilovoltage intrafraction monitoring (KIM) (bottom row) were compared with the planned dose without motion (top row).

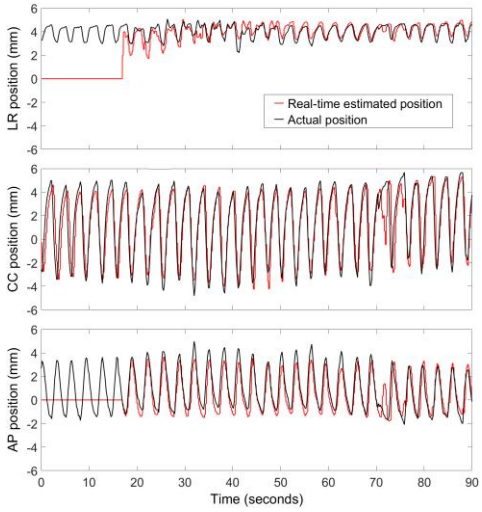

Figure 2. Actual (black) and real-time estimated (red) tumor position used for MLC tracking in the left-right (LR), cranio-caudal (CC) and anterior-posterior (AP) directions during the first field at a fraction (Patient 5, fraction 2).

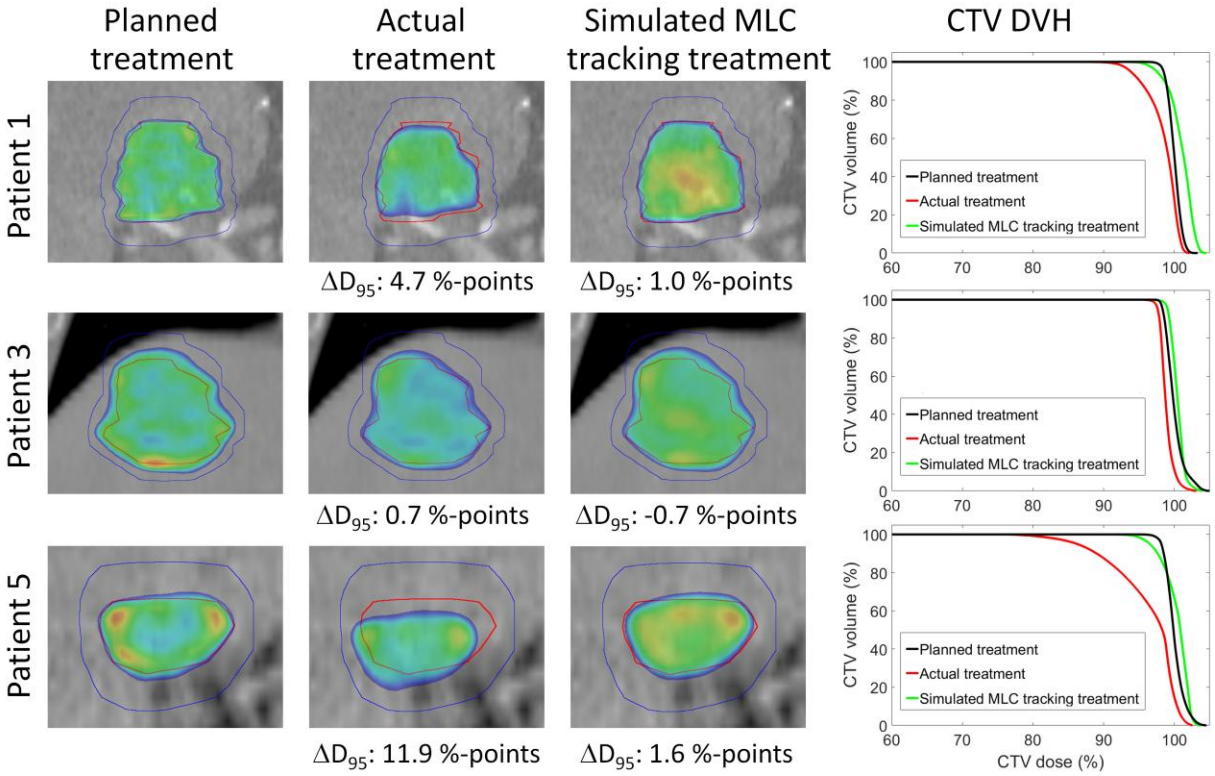

Figure 3. Examples of doses. Dose distributions and CTV dose volume histograms (DVH) as planned and delivered in the actual non-tracking treatments and simulated MLC tracking treatments for three patients. The doses are

accumulated over all three fractions and shown in the coronal plane through the center of the CTV (red structure) and PTV (blue) with a dose color wash range of 95-105% dose.

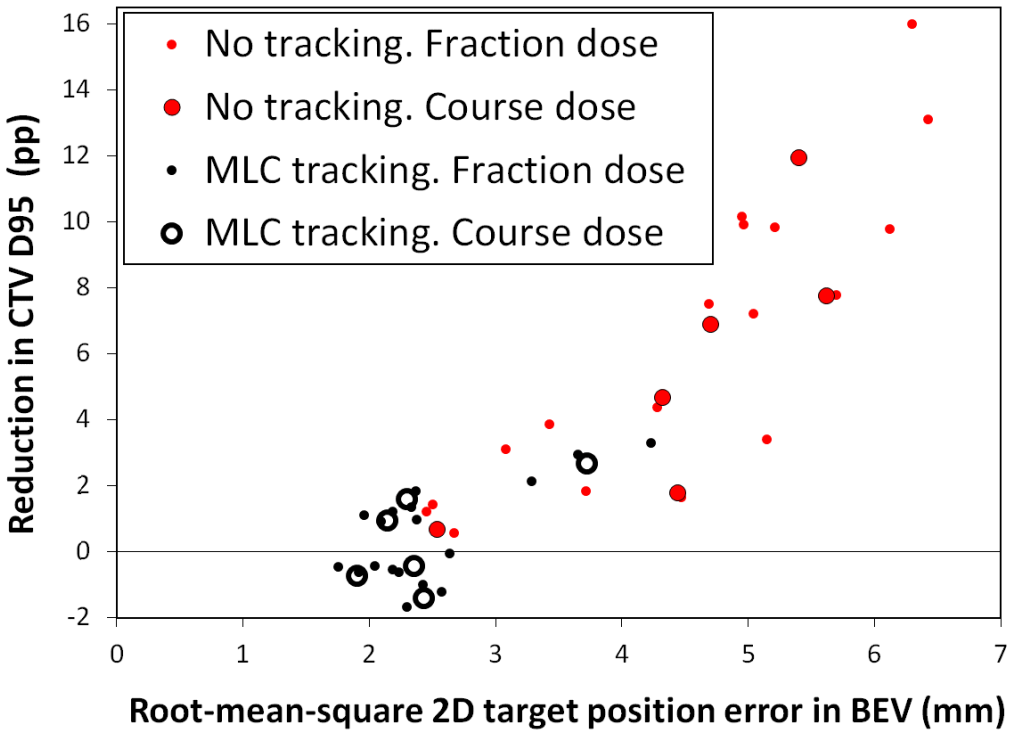

Figure 4. Relation between geometric and dosimetric errors. Percentage point (pp) reduction in CTV D95 versus the root-mean-square 2D target position error in beam's eye view (BEV) with (black) and without (red) MLC tracking for individual treatment fractions (small circles) and treatment courses (large circles).

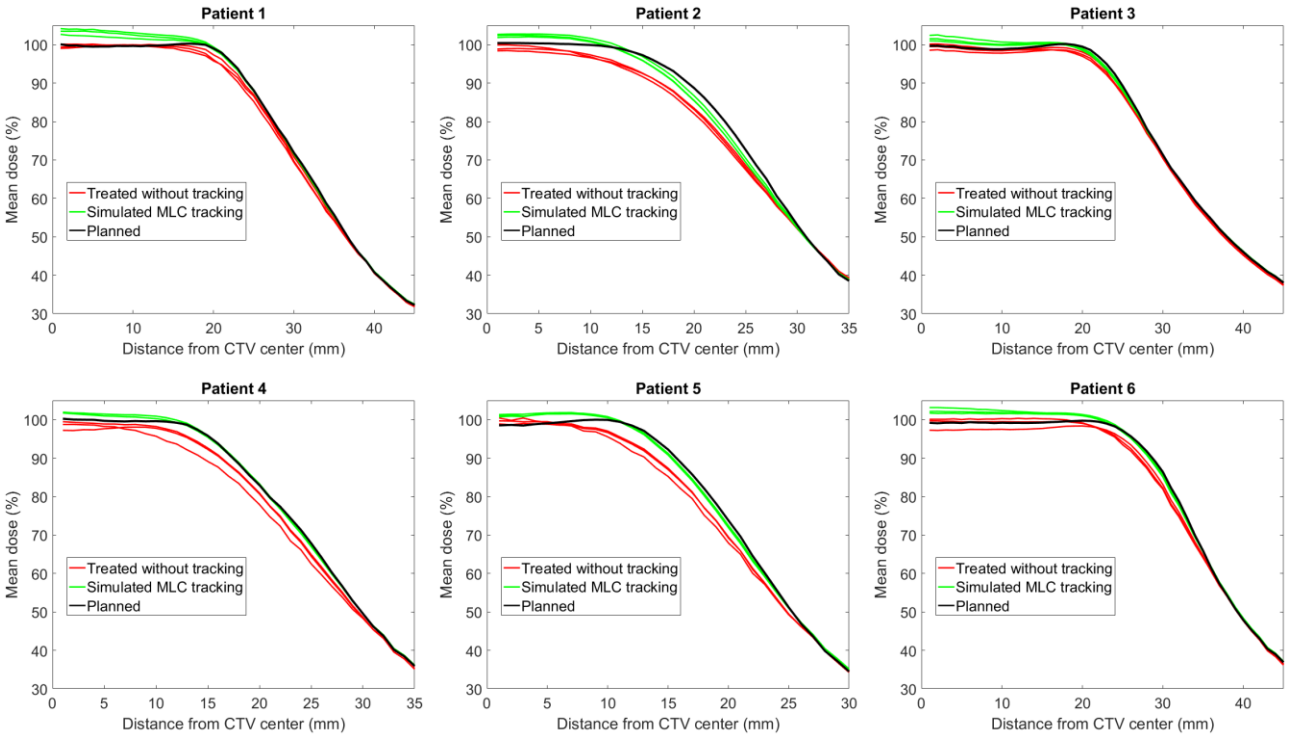

Figure 5. Radial dose distributions. Mean dose as function of radial distance from the CTV center as planned (black) and delivered at each fraction with (green) and without (red) MLC tracking.

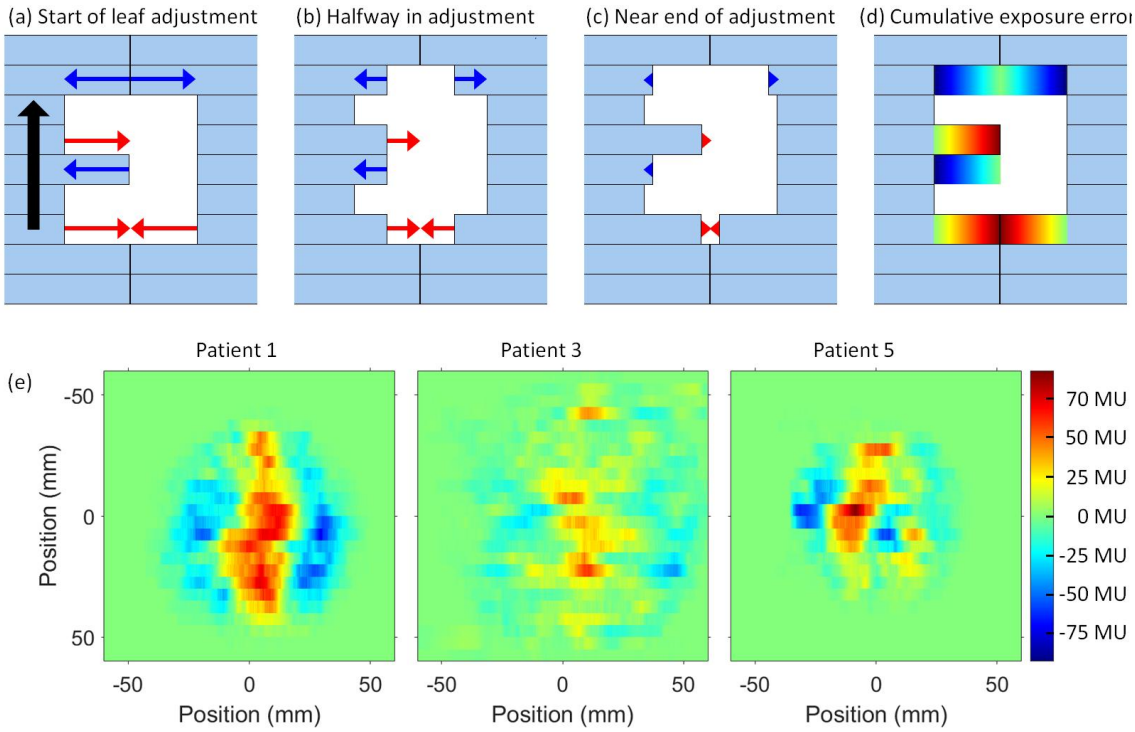

Figure 6. Top: MLC tracking of target motion perpendicular to the MLC leaves. When the target moves one leaf width along the black arrow the MLC leaves will be extended and retracted as indicated by red and blue arrows, respectively. The arrows in (a)-(c) show the not yet performed leaf adjustment, i.e. the MLC exposure error caused by the finite duration of the leaf adjustment. The red and blue arrows represent over-exposed and under-exposed areas, respectively. (d) The cumulative exposure error of the MLC adjustments in (a)-(c) with blue, green and red representing under-exposure, correct exposure and over-exposure, respectively. (e) The cumulative MLC exposure error of MLC adjustments during the simulated MLC tracking treatments for three patients. The MLC exposure errors were cumulated over all arc fields at each fraction and averaged over all three fractions. The unit is monitor units (MU).

References:

1. Blomgren H, Lax I, Näslund I, et al. Stereotactic high dose fraction radiation therapy of extracranial tumors using an accelerator: Clinical experience of the first thirty-one patients. *Acta oncologica* 1995;34:861-870.

2. Lax I, Blomgren H, Naslund I, et al. Stereotactic radiotherapy of malignancies in the abdomen. Methodological aspects. *Acta Oncol* 1994;33:677-83.

3. Petrelli F, Comito T, Barni S, et al. Stereotactic body radiotherapy for colorectal cancer liver metastases: A systematic review. *Radiother Oncol* 2018;129:427-434.

4. Rim CH, Kim HJ, Seong J. Clinical feasibility and efficacy of stereotactic body radiotherapy for hepatocellular carcinoma: A systematic review and meta-analysis of observational studies. *Radiother Oncol* 2019;131:135-144.

5. Poulsen PR, Worm ES, Petersen JB, et al. Kilovoltage intrafraction motion monitoring and target dose reconstruction for stereotactic volumetric modulated arc therapy of tumors in the liver. *Radiother Oncol* 2014;111:424-430.

6. Worm ES, Hoyer M, Hansen R, et al. A prospective cohort study of gated stereotactic liver radiation therapy using continuous internal electromagnetic motion monitoring. *Int J Radiat Oncol Biol Phys* 2018;101:366-375.

7. Nankali S, Worm ES, Hansen R, et al. Geometric and dosimetric comparison of four intrafraction motion adaptation strategies for stereotactic liver radiotherapy. *Phys Med Biol* 2018;63:145010.

8. Bibault J-E, Dewas S, Vautravers-Dewas C, et al. Stereotactic body radiation therapy for hepatocellular carcinoma: prognostic factors of local control, overall survival, and toxicity. *PLOS One* 2013;8:e77472e.

9. Depuydt T, Poels K, Verellen D, et al. Treating patients with real-time tumor tracking using the Vero gimbaled linac system: Implementation and first review. *Radiother Oncol* 2014;112;343-351.

10. Keall PJ, Colvill E, O'Brien R, et al. The first clinical implementation of electromagnetic transponder-guided MLC tracking. *Med Phys* 2014;41:020702.

11. Booth JT, Caillet V, Hardcastle N, et al. The first patient treatment of electromagnetic-guided real time adaptive radiotherapy using MLC tracking for lung SABR. *Radiother Oncol* 2016;121:19-25.

12. Keall PJ, Nguyen DT, O'Brien R, et al. The first clinical implementation of real-time image-guided adaptive radiotherapy using a standard linear accelerator. *Radiother Oncol* 2018;127:6-11.

13. Hoyer M, Roed H, Hansen AT, et al. Phase II study on stereotactic body radiotherapy of colorectal metastases. *Acta Oncol* 2006;45:823-830.

14. Poulsen PR, Cho B, Keall PJ. A method to estimate mean position, motion magnitude, motion correlation, and trajectory of a tumor from cone-beam CT projections for image-guided radiotherapy. *Int J Radiat Oncol Biol Phys* 2008;72:1587-96.

15. Toftegaard J, Hansen R, Ravkilde T, et al. An experimentally validated couch and mlc tracking simulator used to investigate hybrid couch-MLC tracking. *Med Phys* 2017;44:798-809.

16. Fledelius W, Keall PJ, Cho B, et al. Tracking latency in image-based dynamic MLC tracking with direct image access. *Acta Oncol* 2011;50:952-959.

17. Poulsen PR, Fledelius W, Cho B, et al. Image-based dynamic multileaf collimator tracking of moving targets during intensity-modulated arc therapy. *Int J Radiat Oncol Biol Phys* 2012;83:e265-71.

18. Hansen R, Ravkilde T, Worm ES, et al. Electromagnetic guided couch and multileaf collimator tracking on a TrueBeam accelerator. *Med Phys* 2016: 43; 2387-2398.

19. Ruan D. Kernel density estimation-based real-time prediction for respiratory motion. *Phys Med Biol*. 2010;55:1311–1326.

20. Keall PJ, Aun Ng J, O'Brien R, et al. The first clinical treatment with kilovoltage intrafraction monitoring (KIM): A real-time image guidance method. *Med Phys* 2015;42:354-8.

21. Nguyen DT, O'Brien R, Kim JH, et al. The first clinical implementation of a real-time six degree of freedom target tracking system during radiation therapy based on kilovoltage intrafraction monitoring (KIM). *Radiother Oncol* 2017;123:37-42.

22. Poulsen PR, Schmidt ML, Keall P, et al. A method of dose reconstruction for moving targets compatible with dynamic treatments. *Med Phys* 2012;39:6237-46.

29. Ravkilde T, Skouboe S, Hansen R, et al. First online real-time evaluation of motion-induced 4D dose errors during radiotherapy delivery. *Med Phys* 2018;45:3893-3903.

24. Worm ES, Hoyer M, Fledelius W, et al. Variations in magnitude and directionality of respiratory target motion throughout full treatment courses of stereotactic body radiotherapy for tumors in the liver. *Acta Oncol* 2013;52:1437-44.

25. Murtaza G, Toftegaard J, Khan EU, et al. Volumetric modulated arc therapy with dynamic collimator rotation for improved multileaf collimator tracking of the prostate. *Radiother Oncol* 2017;122:109-115.

26. Falk M, Larsson T, Keall P, et al. The dosimetric impact of inversely optimized arc radiotherapy plan modulation for real-time dynamic mlc tracking delivery. *Med Phys* 2012;39:1588-94.

27. Fast MF, Nill S, Bedford JL, et al. Dynamic tumor tracking using the elekta agility MLC. *Med Phys* 2014;41:111719.

28. Ehrbar S, Schmid S, Johl A, et al. Comparison of multi-leaf collimator tracking and treatment-couch tracking during stereotactic body radiation therapy of prostate cancer. *Radiother Oncol* 2017;125:445-452.

29. Colvill E, Poulsen PR, Booth JT, et al. DMLC tracking and gating can improve dose coverage for prostate VMAT. *Med Phys* 2014;41:091705.

30. Kamerling CP, Fast MF, Ziegenhein P, et al. Real-time 4D dose reconstruction for tracked dynamic MLC deliveries for lung SBRT. *Med Phys* 2016;43:6072.

31. Skouboe S, Ravkilde T, Bertholet J, et al. First clinical real-time motion-including tumor dose reconstruction during radiotherapy delivery. *Radiother Oncol* 2019;139:66-71